AFRL-ML-WP-TP-2007-504

ACCURATE EVALUATION OF NONLINEAR ABSORPTION COEFFICIENTS IN InAs, InSb AND HbCdTe ALLOYS (POSTPRINT)

Shekhar Guha

Hardened Materials Branch
Survivability and Sensor Materials Division

NOVEMBER 2006

AIR FORCE RESEARCH LABORATORY
MATERIALS AND MANUFACTURING DIRECTORATE
WRIGHT-PATTERSON AIR FORCE BASE, OH 45433-7750
AIR FORCE MATERIEL COMMAND
UNITED STATES AIR FORCE

NOTICE AND SIGNATURE PAGE

Using Government drawings, specifications, or other data included in this document for any purpose other than Government procurement does not in any way obligate the U.S. Government. The fact that the Government formulated or supplied the drawings, specifications, or other data does not license the holder or any other person or corporation; or convey any rights or permission to manufacture, use, or sell any patented invention that may relate to them.

This report was cleared for public release by the Air Force Research Laboratory Wright Site (AFRL/WS) Public Affairs Office and is available to the general public, including foreign nationals. Copies may be obtained from the Defense Technical Information Center (DTIC) (http://www.dtic.mil).

AFRL-ML-WP-TP-2007-504 HAS BEEN REVIEWED AND IS APPROVED FOR PUBLICATION IN ACCORDANCE WITH ASSIGNED DISTRIBUTION STATEMENT.

*//Signature//

SHEKHAR GUHA, Ph.D.
Agile IR Limiters
Exploratory Development
Hardened Materials Branch

//Signature//

MARK S. FORTE, Acting Chief
Hardened Materials Branch
Survivability and Sensor Materials Division

//Signature//

TIM J. SCHUMACHER, Chief
Survivability and Sensor Materials Division

This report is published in the interest of scientific and technical information exchange, and its publication does not constitute the Government's approval or disapproval of its ideas or findings.

*Disseminated copies will show "//Signature//" stamped or typed above the signature blocks.

REPORT DOCUMENTATION PAGE

Form Approved
OMB No. 0704-0188

1. REPORT DATE *(DD-MM-YY)*	2. REPORT TYPE	3. DATES COVERED *(From - To)*
November 2006	Journal Article Postprint	

4. TITLE AND SUBTITLE
ACCURATE EVALUATION OF NONLINEAR ABSORPTION COEFFICIENTS IN InAs, InSb AND HbCdTe ALLOYS (POSTPRINT)

5a. CONTRACT NUMBER
In-house

5b. GRANT NUMBER

5c. PROGRAM ELEMENT NUMBER
62102F

6. AUTHOR(S)
Srinivasan Krishnamurthy and Zhi Gang Yu (SRI International)
Leonel P. Gonzalez (General Dynamics Information Technology, Inc.)
Shekhar Guha (AFRL/MLPJ)

5d. PROJECT NUMBER
4348

5e. TASK NUMBER
RG

5f. WORK UNIT NUMBER
M08R1000

7. PERFORMING ORGANIZATION NAME(S) AND ADDRESS(ES)

SRI International
333 Ravenswood Avenue
Menlo Park, CA 94025

General Dynamics Information Technology, Inc.
5100 Springfield Pike, Suite 509
Dayton, OH 45431-1264

Hardened Materials Branch (AFRL/MLPJ)
Survivability and Sensor Materials Division
Materials and Manufacturing Directorate
Wright-Patterson Air Force Base, OH 45433-7750
Air Force Materiel Command
United States Air Force

8. PERFORMING ORGANIZATION REPORT NUMBER
AFRL-ML-WP-TP-2007-504

9. SPONSORING/MONITORING AGENCY NAME(S) AND ADDRESS(ES)
Air Force Research Laboratory
Materials and Manufacturing Directorate
Wright-Patterson Air Force Base, OH 45433-7750
Air Force Materiel Command
United States Air Force

10. SPONSORING/MONITORING AGENCY ACRONYM(S)
AFRL/MLPJ

11. SPONSORING/MONITORING AGENCY REPORT NUMBER(S)
AFRL-ML-WP-TP-2007-504

12. DISTRIBUTION/AVAILABILITY STATEMENT
Approved for public release; distribution unlimited.

13. SUPPLEMENTARY NOTES
Journal article published in Journal of Applied Physics, Vol. 101 (2007).

 PAO Case Number: AFRL/WS 06-2511, 23 Oct 2006.

14. ABSTRACT
We present a full band structure calculation of temperature- and wavelength-dependent two-photon absorption (TPA) coefficients and free carrier absorption (FCA) cross sections in InAs, InSb, and $Hg_{1-x}Cd_xTe$ alloys. Although the wavelength dependence of the TPA coefficients agrees well with Wherrett expression, the accurately calculated values are smaller by a factor of 1.2 to 2.5. In addition, the TPA coefficient depends sensitively on the photoexcited carrier density in small gap material. The FCA is dominated by holes. The FCA cross section is independent of carrier density, but is strongly dependent on temperature. The calculated coefficients and lifetimes are fitted to closed form expressions and used in solving the rate equation to obtain the transmitted pump and probe intensities as functions of incident intensity and sample thickness. The calculated pump transmission and time-dependent probe transmission in InAs agree very well with the measured values.

15. SUBJECT TERMS
Two-photon absorption (TPA), free carrier absorption (FCA)

16. SECURITY CLASSIFICATION OF:			17. LIMITATION OF ABSTRACT:	18. NUMBER OF PAGES	19a. NAME OF RESPONSIBLE PERSON (Monitor)
a. REPORT	b. ABSTRACT	c. THIS PAGE			Shekhar Guha
Unclassified	Unclassified	Unclassified	SAR	18	19b. TELEPHONE NUMBER *(Include Area Code)* N/A

Standard Form 298 (Rev. 8-98)
Prescribed by ANSI Std. Z39-18

Accurate evaluation of nonlinear absorption coefficients in InAs, InSb, and HgCdTe alloys

Srinivasan Krishnamurthy[a] and Zhi Gang Yu
SRI International, 333 Ravenswood Avenue, Menlo Park, California 94025

Leonel P. Gonzalez
General Dynamics Information Technology, Dayton, Ohio 45433

Shekhar Guha
Air Force Research Laboratory, Materials and Manufacturing Directorate, Wright Patterson Air Force Base, Ohio 45433

(Received 25 October 2006; accepted 15 February 2007; published online 6 June 2007)

We present a full band structure calculation of temperature- and wavelength-dependent two-photon absorption (TPA) coefficients and free carrier absorption (FCA) cross sections in InAs, InSb, and $Hg_{1-x}Cd_xTe$ alloys. The wavelength dependence of the TPA coefficients agrees well with a widely used analytical expression. However, the magnitudes of the TPA coefficients obtained here are smaller by a factor of 1.2–2.5 than the analytical values. In addition, the TPA coefficient is found to depend sensitively on the photoexcited carrier density in small gap materials. The FCA is found to arise predominantly from hole absorption. The FCA cross section is found to be independent of the carrier density, but is strongly dependent on the temperature. The calculated TPA, FCA coefficients, and lifetimes are fitted to closed-form expressions and are used in solving the rate equations to obtain the transmitted pump and probe intensities as functions of incident intensity and sample thickness. The calculated pump transmission and time-dependent probe transmission in InAs agree very well with the measured values. © *2007 American Institute of Physics*.
[DOI: 10.1063/1.2718874]

INTRODUCTION

The nonlinear optical absorption and refraction properties affect the propagation of high intensity light through transparent materials.[1,2] Several physical mechanisms, including two-photon absorption, free-carrier absorption, and thermal and free carrier refractions, are responsible for nonlinear properties.[3–6] Both theory and experiments are constantly being improved to accurately evaluate nonlinear absorption and refraction coefficients.[7–22] When the energy of high intensity incident photons is more than half of the band gap energy of the semiconductor, the electrons in the valence band (VB) absorb two photons to reach the unoccupied states in the conduction band (CB). Then the photoexcited electrons and holes further absorb a photon with or without the assistance of a phonon, causing further reduction in intensity as the light travels through the material. Since the two-photon absorption (TPA) plays a vital role in initiating the nonlinearity in the material, a number of studies have been undertaken to accurately evaluate the TPA coefficient. However, the extraction of TPA values from these experiments often depended on the ability to control other factors that simultaneously affected the nonlinear absorption. Consequently, the extracted values varied substantially.[7–10,15,18–21] On the theoretical side, Wherrett's expression[12] with nonparabolic correction[11] was used widely. Later it was modified, and the interaction matrix element was parametrized based on the ability of the $\mathbf{k}\cdot\mathbf{p}$ models to successfully predict the trends in various semiconductors.[14–17] This expression served an excellent role in providing qualitative trends and giving approximate values for the TPA coefficients used in understanding light propagation. However, an accurate evaluation, with full band structures and matrix elements included, of TPA coefficient made recently[22,23] has revealed that the calculated values differ substantially, by as much as a factor of 5, from those given by the simple analytical formula.

Light propagation is further affected by free carrier absorption (FCA), in which the photogenerated photoexcited carriers absorb photons. The cross section for the free carrier absorption, defined as the ratio of free carrier absorption coefficient to the free carrier density, is generally assumed to be a constant in light propagation studies.[3–6] However, in our detailed calculations we found that the cross section is strongly dependent on wavelength and temperature. We have carried out these calculations with full band structures for InSb, InAs, and $Hg_{1-x}Cd_xTe$ alloys. The band gap energies of InAs and InSb at 300 K are 0.35 and 0.175 eV, respectively.

In this paper, we first provide a brief description of the band structures, the quasi-Fermi energies, and the nonlinear absorption coefficients (TPA and FCA). The wavelength and carrier density dependences of the TPA and FCA coefficients in InAs, InSb, and HgCdTe alloys are reported. The calculated values of TPA and FCA in InSb, InAs, and HgCdTe alloys (with $x=0.24$ and $x=0.34$) are also fitted to the simple analytical form so they can be used easily in light propagation modeling.[3–6,24] These values are used in obtaining a solution to the rate equation that describes the light propagation through InAs. The results are then compared with the information found in the experiments.

[a]Electronic mail: srini@sri.com

THEORY

Second-order perturbation theory is used to calculate the TPA and FCA coefficients[22] and the Auger and radiative recombination lifetimes.[25–27] The dipole matrix elements required to study light interaction with matter and the scattering matrix elements required in lifetime calculations are calculated from the underlying band structures. Care is given to describe the occupancy of initial and final states with appropriate Fermi-Dirac distributions and to include an accurate sum over crystal wave vectors spanning the entire Brillouin zone (BZ).

Band structures

The calculations reported here are based on a hybrid pseudopotential tight-binding Hamiltonian.[28] In this formalism, the tight-binding Hamiltonian contains two parts. The dominant part is derived from the empirical pseudopotential and includes all long-range interactions. A short-range empirical Hamiltonian is added to fine tune the calculated band structure so that it agrees with the measured energy gaps and effective masses at various symmetry points in the BZ. In the sp^3 basis, with the spin-orbit coupling included, the Hamiltonian takes the 16×16 matrix form. In the case of alloys, we find that the correction to bands from the alloy disorder is small near the band edge, and hence, the virtual crystal approximation can be used to obtain the alloy band structures. The resulting Hamiltonian matrix is diagonalized to yield the eigenvalues (energies) and eigenvectors (wave functions).

Since high intensity light absorbed in a material can raise the material temperature substantially above room temperature, band structures over a wide range of temperatures from 77 K up to ~500 K need to be used. Although the temperature (T) dependence of the matrix elements can be included[29] for the calculation of the band structure, those calculations are extremely time-consuming, particularly when the integration over the full BZ is required for lifetime calculations. Here, as an alternative, the effect of T on the $Hg_{1-x}Cd_xTe$ alloy band structure is included indirectly as follows. First, for a given T and Cd concentration x, the band gap E_g in eV is determined from the widely used relationship[30] $-0.302+1.93x+5.35\times10^{-4}\ (1-2x)^*T-0.81x^2+0.832x^3$. We then adjust the value of x in our zero-temperature Hamiltonian to x' to get the band gap of E_g. The zero-temperature Hamiltonian with the value of x' is then used in further calculations. In the case of InAs and InSb compounds, the parameters of the short-range empirical Hamiltonian are adjusted at each temperature to yield the band gap in eV given by $0.415-2.76\times10^{-4}T^2/(T+83)$ and $0.24-6\times10^{-4}T^2/(T+500)$, respectively.[31,32] The calculated band gap energy as a function of T is shown as a dashed line in Fig. 1 for (a) InAs, (b) $Hg_{0.66}Cd_{0.34}Te$, (c) InSb, and (d) $Hg_{0.76}Cd_{0.24}Te$. We see that the band gap decreases with T in InAs and InSb, but increases in HgCdTe alloys.

Fermi level

The study of electron-photon interaction requires the knowledge of the electron density and its distribution. The Boltzmann distribution is often used. However, at high temperatures and for small gap materials, the bands are nearly or fully degenerate and the Fermi-Dirac (FD) distribution function,

$$f(E,E_f)=[1+e^{(E-E_f)/k_BT}]^{-1}, \tag{1}$$

needs to be used, where k_B is the Boltzmann constant. The equilibrium Fermi level (FL) or Fermi energy E_f in Eq. (1) is obtained from the charge neutrality condition that the total positive charges (the sum of equilibrium hole density p_0 and ionized donor density N_D^+) equals the total negative charges (the sum of equilibrium electron density n_0 and ionized acceptor density N_A^-).[33] The quantities n_0, p_0, N_D^+, and N_A^-, in turn, depend on the Fermi energy as follows:

$$N_D^+=N_D[1+ge^{(E_f-E_D)/k_BT}]^{-1},$$
$$N_A^-=N_A[1+ge^{(E_A-E_f)/k_BT}]^{-1}, \tag{2}$$

$$n_0=2\int_{E_c}^{\infty}\rho_c(E-E_c)f(E,E_f)dE,$$

$$p_0=2\int_{-\infty}^{E_v}\rho_v(E-E_v)f(E,E_f)dE, \tag{3}$$

$$\rho_{c,v}=\frac{1}{\Omega}\sum_{\mathbf{k}}\delta(E_{c,v}^{\mathbf{k}}-E),$$

where Ω is the crystal volume, the degeneracy factor g is 2 for CB and 4 for VB, and E_c and E_v are the band energies at CB minimum and VB maximum, respectively. In the special case where the material is intrinsic ($N_D=N_A=0$), the FL is denoted by E_f^i and the corresponding carrier density ($n_0=p_0$) is denoted by n_i. The calculated E_f^i is shown by the dotted line in Fig. 1 for (a) InAs, (b) $Hg_{0.66}Cd_{0.34}Te$, (c) InSb, and (d) $Hg_{0.76}Cd_{0.24}Te$. All energies are measured with respect to the top of the VB at that temperature. At low temperature, the E_f^i is near the midgap. Owing to the difference in the effective masses of electrons and holes, the FL moves closer to the CB edge (shown as a dashed line) with an increase in T. In the case of InSb, we see that the FL lies above the bottom of the CB at high temperature, making the material fully degenerate. In HgCdTe alloys, the band gap increases with T and hence the intrinsic FL continues to lie below the CB for all the temperatures considered here. The corresponding intrinsic carrier density n_i obtained from Eq. (3) is plotted in Fig. 2 for all four materials. The intrinsic carrier density increases with T but decreases with E_g and varies approximately as $\exp(-E_g/2k_BT)$. This behavior is clearly seen in Fig. 2. Recently, the variable Hall studies, in combination with multiple carrier analysis, have demonstrated the ability to yield an accurate measurement of the carrier density in doped samples.[34–36] The carrier densities calculated using our band structures were found to be in excellent agreement with these measurements.[25]

Under high intensity light illumination, photoexcited electron density (Δn) and hole density (Δp) are created, with $\Delta n=\Delta p$, which can be far larger than the equilibrium carrier density n_0 and p_0. Consequently, the TPA, FCA coefficients,

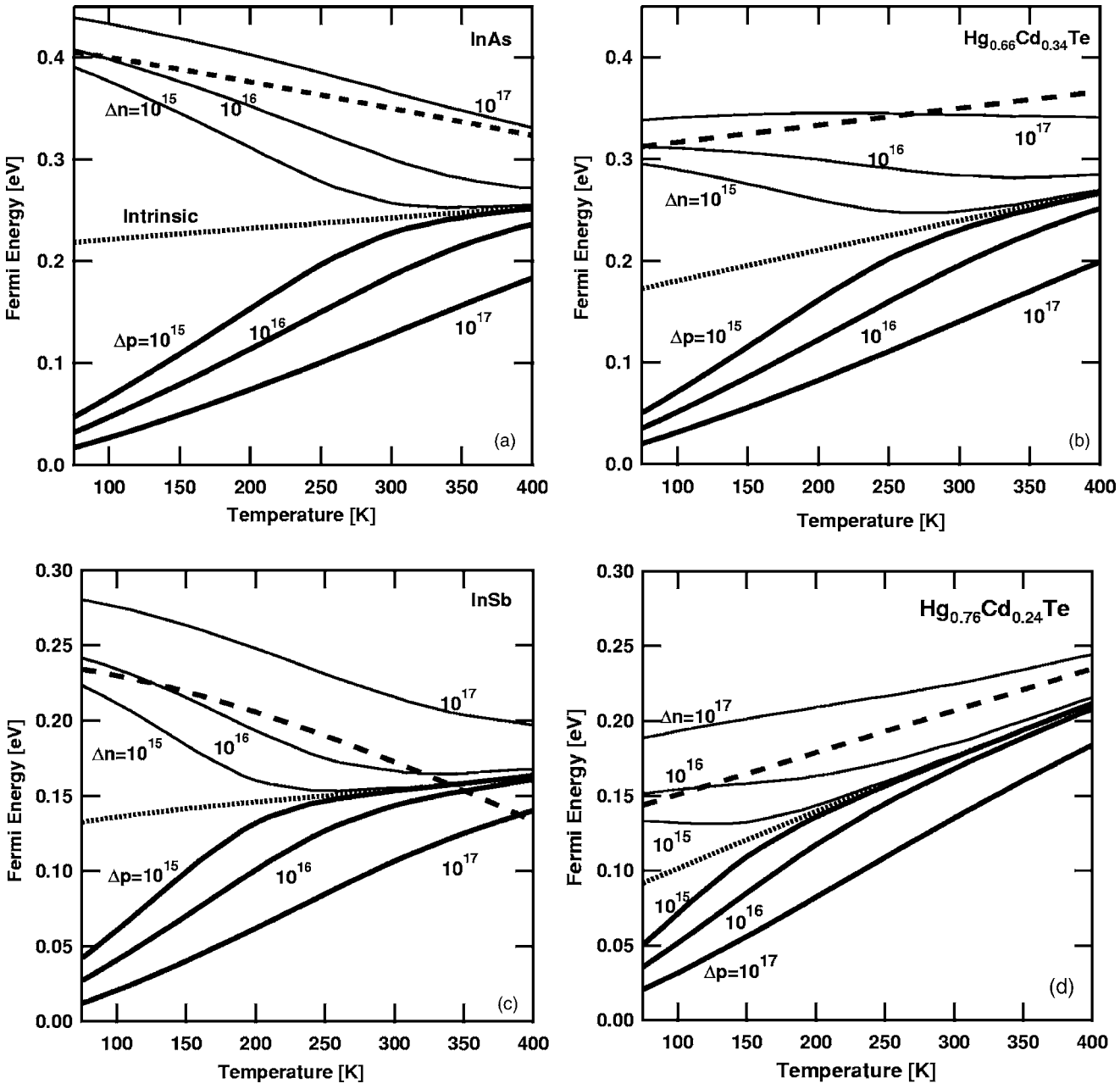

FIG. 1. Variation of energy gap (dashed line) and intrinsic Fermi energy (dotted line) with temperature. Also shown are electron quasi-Fermi energy (thin solid line) and hole quasi-Fermi energy (thick solid line) for various photoexcited carrier densities ($\Delta n = \Delta p$).

and lifetime calculations have to be carried out not only under degenerate conditions but also under nonequilibrium condition, in which the electrons in the CB and the holes in the VB have different Fermi energies. This quasi-Fermi energy for electrons (E_f^c) and holes (E_f^v) is determined from the following conditions:

$$n_0 + \Delta n = 2\int_{E_c}^{\infty} \rho_c(E - E_c) f(E, E_f^c) dE,$$
$$p_0 + \Delta p = 2\int_{-\infty}^{Ev} \rho_c(E - E_v) f(E, E_f^v) dE. \quad (4)$$

Assuming that the material is intrinsic, we have calculated the quasi-FLs for various values of the photoexcited carrier density using Eq. (4). Also shown in Fig. 1 are calculated electron (thin solid line) and hole (thick solid line) Fermi energies as functions of the lattice temperature and excited carrier density. When the photoexcited carrier density ($\Delta n = \Delta p$) becomes appreciably larger than the intrinsic carrier density n_i at that T, the quasi-FL for electrons (holes) is closer to the CB (VB). However, when the n_i is larger than Δn or Δp, the quasi-FLs merge with the intrinsic FL as shown in Fig. 1. The charge carrier distribution described by the FD function differs considerably from that described by the Maxwell-Boltzmann function when the quasi-FLs are closer to the band edge. Consequently, we see from Fig. 1 that the quasi-FLs play a major role even in systems with moderate excited carrier densities at low T and in systems with large densities at high T, in general.

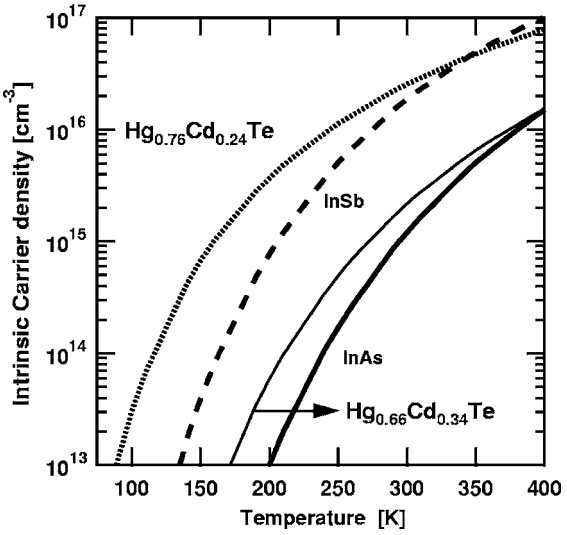

FIG. 2. Variation of intrinsic carrier density with temperature.

Two-photon absorption

Electrons in the heavy-hole (HH) and light-hole (LH) valence bands absorb two photons to reach the CB states. In the second-order perturbation theory, the absorption rate is proportional to the occupation of the initial state in the VB, availability of the final state in the CB, and the dipole matrix element between the VB and CB states at a given crystal momentum. Explicitly, the expression for TPA coefficient β is

$$\beta = \frac{1}{\pi c}\left(\frac{2\pi e}{m}\right)^4 \frac{1}{(\omega n)^3} \sum_{\alpha\beta\mathbf{k}} [1 - f(E_\beta^{\mathbf{k}}, E_f^\beta)] \times |M_{\alpha\beta}^{\mathbf{k}}|^2 f(E_\alpha^{\mathbf{k}}, E_f^\alpha)\, \delta(E_\alpha^{\mathbf{k}} - E_\beta^{\mathbf{k}} + 2\hbar\omega), \quad (5)$$

$$M_{\alpha\beta}^{\mathbf{k}} = \sum_{\beta'} \sum_{jj'} \frac{\langle \phi_\beta^{\mathbf{k}} | \mathbf{e}_{j'} \cdot \mathbf{p} | \phi_{\beta'}^{\mathbf{k}} \rangle \langle \phi_{\beta'}^{\mathbf{k}} | \mathbf{e}_{\mathbf{j}} \cdot \mathbf{p} | \phi_\alpha^{\mathbf{k}} \rangle}{\mathbf{E}_\alpha^{\mathbf{k}} - \mathbf{E}_{\beta'}^{\mathbf{k}} + \hbar\omega}, \quad (6)$$

where $E_\beta^{\mathbf{k}}(\phi_\beta^{\mathbf{k}})$ is the electron energy (wave function) in band β at the wave vector $\mathbf{k}$ in the BZ, e and m are the free electron charge and mass, n is the real part of the refractive index, $\mathbf{p}$ is the electric dipole vector, $\mathbf{e_j}$ is the unit vector in the polarization direction of light, and $\hbar\omega$ is the photon energy. The distribution function for the electrons $f(E_\beta^{\mathbf{k}})$ given by Eq. (1) uses appropriate quasi-Fermi energies E_f^v and E_f^c depending on whether β denotes a valence or a conduction band. In Eq. (5), α and β denote respectively the initial and final states in any occupied VB and any unoccupied CB that satisfies the energy conservation condition specified by the δ function. The sum over $\mathbf{k}$ is performed over the entire BZ. A careful analysis shows that the intermediate state β' can be any of the unoccupied CB state and one VB state from which the electron excitation begins. In fact, the leading term of Eq. (6) arises when β' is the same as α In that case, the denominator of Eq. (6) is simply $\hbar\omega$, $\langle \phi_\beta^{\mathbf{k}} | \mathbf{e}_{\mathbf{j}'} \cdot \mathbf{p} | \phi_\alpha^{\mathbf{k}} \rangle$ is nearly a constant for $\mathbf{k}$ close to the BZ center, and $\langle \phi_\alpha^{\mathbf{k}} | \mathbf{e}_{\mathbf{j}'} \cdot \mathbf{p} | \phi_\alpha^{\mathbf{k}} \rangle$ is proportional to $\mathbf{k}$. After substituting for $M_{\alpha\beta}$ in Eq. (5) under the assumption that VB is occupied, CB is unoccupied, and the bands are described in parabolic approximation, it is straightforward to show that β is proportional to $(2\hbar\omega - E_g)^{3/2}/\omega^5$. This functional dependence of β is being widely used in the literature.[6,9,11,12,14–17,20]

We used full band structures to accurately calculate the FD distribution function, band energy, wave functions, and optical matrix elements to obtain β as a function of the photon wavelength λ and T. The calculated β at $T=300$ and 77 K are shown in Fig. 3 for (a) InAs, (b) $Hg_{0.66}Cd_{0.34}Te$, (c) InSb, and (d) $Hg_{0.76}Cd_{0.24}Te$. In all cases considered here, β increases with λ, reaches a maximum, and decreases to zero. The leading term in Eq. (6) varies as ω^{-1} and, consequently, β in Eq. (5) varies as ω^{-5} (or λ^5) β in Fig. 3 increases initially with the wavelength λ. However β is also proportional to the density of states at the excitation energy $(2hc/\lambda - E_g)$ in the conduction band. The density of states decreases when λ is increased. The competition between these two terms results in a maximum in β. When λ is longer than twice the cutoff wavelength λ_g (with $\lambda_g = hc/E_g$), electrons in the VB cannot reach the CB and β drops to zero. The approximate value of λ where the β reaches a maximum can be estimated from Eqs. (5) and (6). In the approximation where the dipole matrix element is proportional to $\mathbf{k}$, the initial state is always occupied, the final state is always empty, and the bands can be described by an effective mass, β from Eqs. (5) and (6) is proportional to $\lambda^5(2hc/\lambda - E_g)^{3/2}$. The maximum of this function occurs when λ is $1.4\lambda_g$. In general, the band structure is not parabolic. In our full calculations, we find that TPA reaches its largest value when λ is approximately $1.5\lambda_g$. This empirical relationship holds well for all four materials and two temperatures considered here.

As the one-photon absorption will start to dominate at wavelengths shorter than the cutoff wavelength for the given T, the values of β are not calculated in that spectral region. In InAs and InSb, the band gap decreases when T is increased and hence the density of states (DOS) at the excitation energy $(2hc/\lambda - E_g)$ increases, resulting in a larger β at higher T. For similar reasons, β in HgCdTe decreases when T is increased. Although the band gaps of InAs and $Hg_{0.66}Cd_{0.34}Te$ at room temperature are equal, notice that β in the HgCdTe alloy is considerably higher than in InAs owing to the difference in their density of states.

For an intrinsic material at low temperature, the initial state is full and the final state is almost empty. However, as discussed in the previous section, the occupancy or availability of the states depends not only on T but also on the excess carrier density. Consequently, the calculated β has a dependence on the photoexcited carrier density, as shown in Fig. 4 at (a) 300 K and (b) 77 K. At 300 K, the intrinsic carrier density in InAs and $Hg_{0.66}Cd_{0.34}Te$ is small because of the large band gap, and the calculated β shows only a slight variation with the photoexcited carrier density. However, in the small gap InSb and $Hg_{0.76}Cd_{0.24}Te$, the intrinsic carrier density is large. Additional photoexcited carriers deplete (fill) the near band edge VB (CB) states. Hence, the occupancy (availability) of the initial (final) state is different from 1 (zero), resulting in a decreased β. We see that the calculated β starts to decrease for the photoexcited carrier densities in excess of mid 10^{16} cm^{-3}. This effect, commonly known as the Moss-Burstein effect, is dominant for small band gap

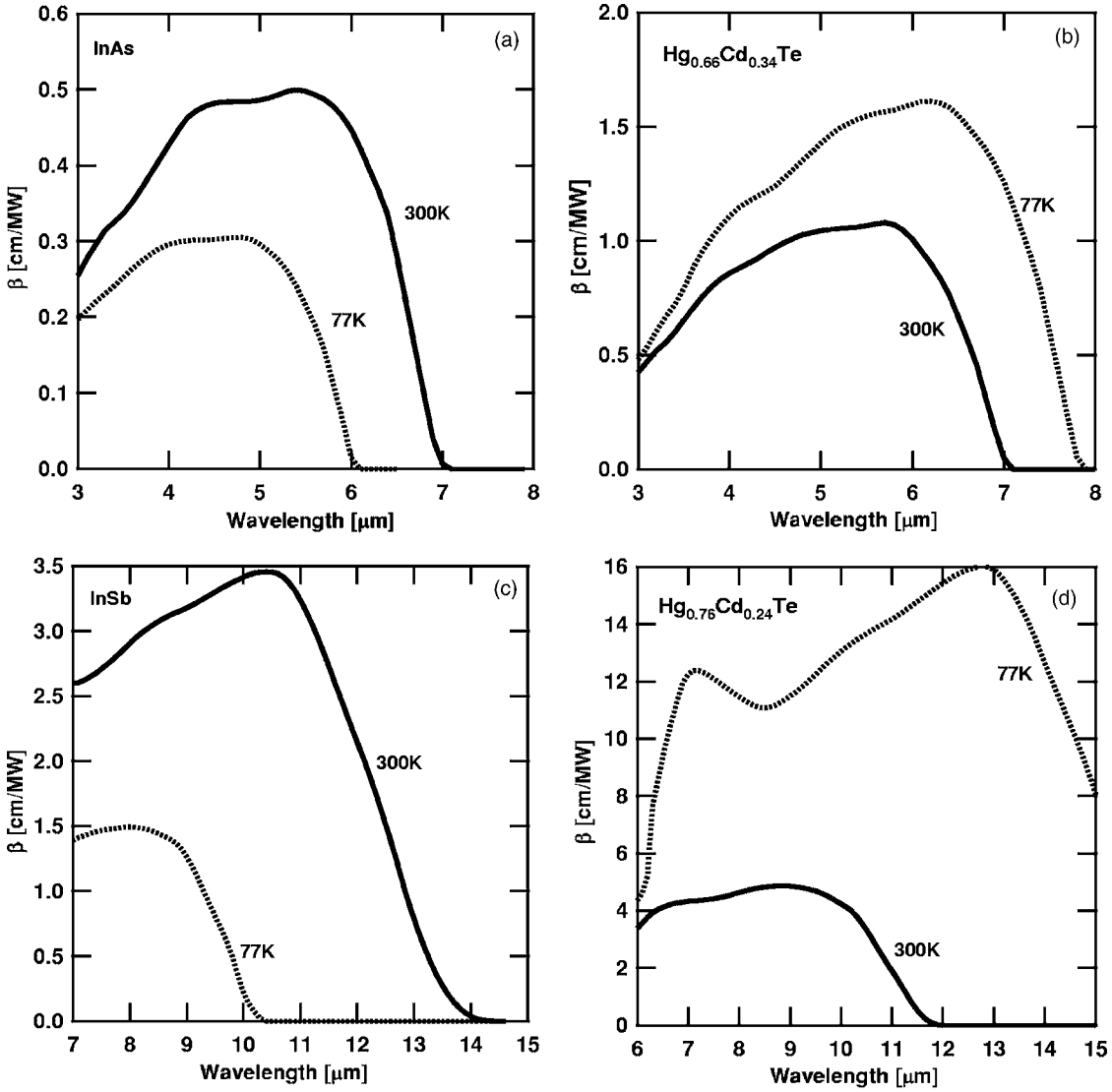

FIG. 3. Two-photon absorption coefficient as a function of wavelength and temperature.

materials and at low T. The β calculated at 77 K shows an even stronger carrier density dependence, as shown in Fig. 4(b).

It is instructive to compare the calculated β to that obtained by most commonly used, but approximate, methods. Qualitatively, the wavelength dependence shown in Fig. 4 agrees well with that predicted by Wherrett's or Van Stryland's expression.[8,11] Our calculated values and those obtained with Van Stryland's expression are given in Table I for two temperatures and wavelengths. We see that our values of β calculated at 4.8 μm and at low carrier density are smaller than those obtained with Van Stryland's expression by a factor of 2.5 for $Hg_{0.66}Cd_{0.34}Te$ and by 1.5 for InAs. Similarly, the values of β calculated at 9.6 μm and low carrier density are smaller by a factor of 2.2 for InSb and by 1.2 for $Hg_{0.74}Cd_{0.26}Te$.

Unlike InAs and InSb, the band gap of the $Hg_{1-x}Cd_xTe$ alloy can be continuously varied from 0 to 1.6 eV by changing Cd concentration. Since this alloy system can be used to study the propagation of light at a number of wavelengths, the wavelength-dependent calculations of β at low carrier densities are carried out as a function of x and are shown in Fig. 5 for (a) $T=300$ K and (b) $T=77$ K. The wavelength dependence is similar in all alloys at both temperatures. However, as the value of x increases, the band gap increases and, consequently, β decreases. Similarly, the band gap increase with temperature also causes the decrease in β. This is clearly seen in Fig. 5. Interestingly, β reaches the maximum when $\lambda \approx 1.5\lambda_g$ for these alloys and temperatures, except for $x=0.2$ alloy at 77 K. The maximum occurs when $\lambda \approx 1.2\lambda_g$. Since the band gap is very small (83 meV) for this alloy at 77 K, the conduction band near the BZ center is mostly linear in $\mathbf{k}$, and not parabolic. For these bands, β is proportional to $\lambda^5(2hc/\lambda - E_g)^2$ and the maximum of this function is at $\lambda \approx 1.2\lambda_g$, in agreement with our calculated value.

Free carrier absorption

The photocarriers excited by the TPA can cause further absorption of light. When a hole is photogenerated in the heavy-hole VB, the electrons in the light-hole VB can absorb one photon and get excited to fill that hole. This direct pro-

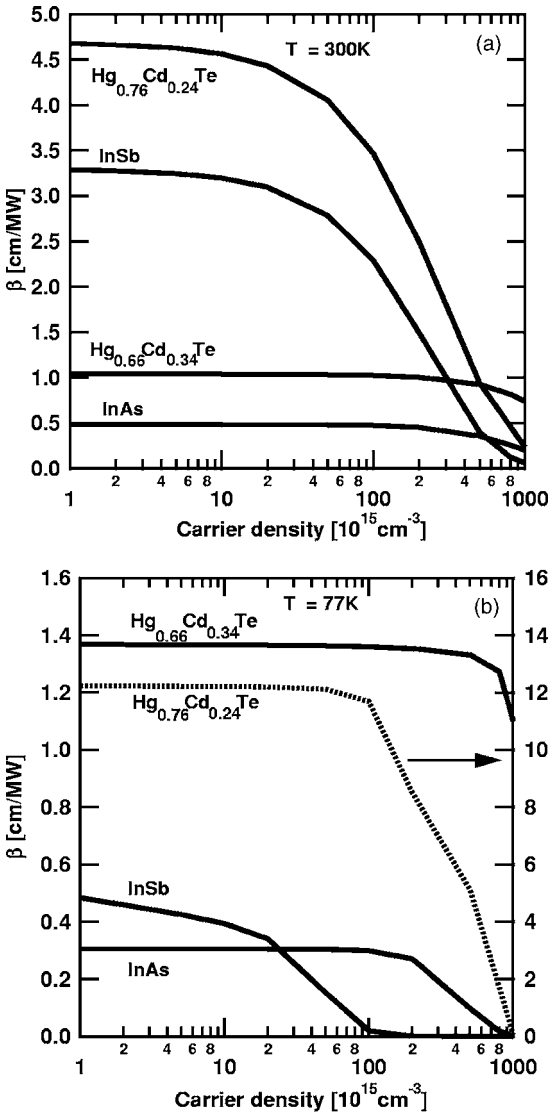

FIG. 4. Two-photon absorption coefficient as a function of excited carrier density Δn at (a) 300 K and (b) 77 K. The right axis in (b) corresponds to $x=0.24$ alloy.

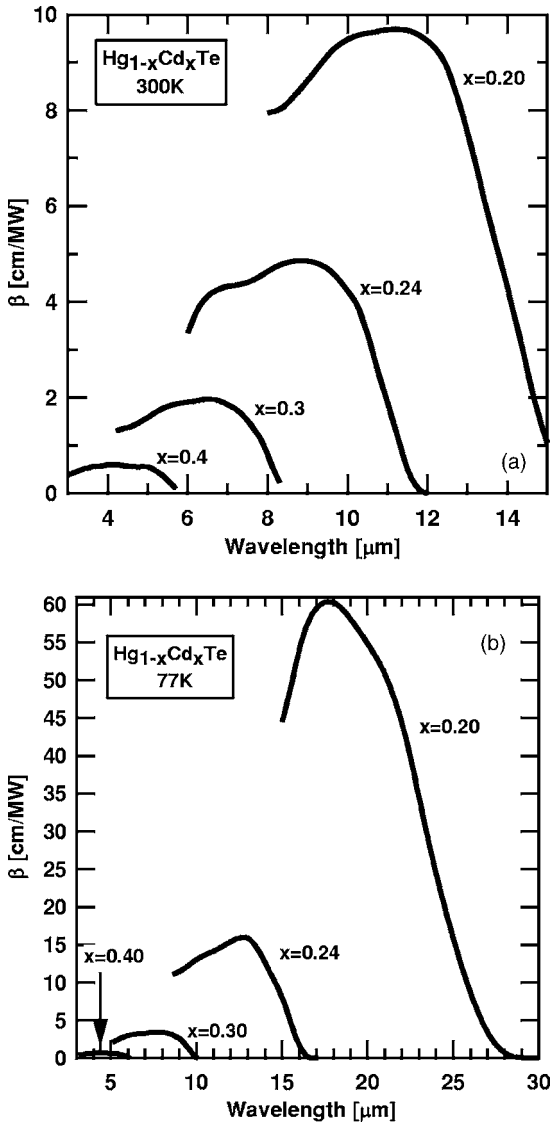

FIG. 5. Two-photon absorption coefficient as a function of wavelength in HgCdTe alloys at (a) 300 K and (b) 77 K.

cess is normally known as FCA by holes. The photogenerated electron in the CB can also absorb a photon through an indirect process. To satisfy the momentum and energy conservation conditions, the photon absorption by conduction electrons should be accompanied by a phonon absorption or emission. The free carrier absorption rate calculated from second-order perturbation theory is used to obtain the FCA coefficient α_f and the FCA cross section σ. Although the basic formalism has been described previously,[22] here the explicit expressions for two contributions—the direct term and the indirect term—are provided. This helps us separate the contributions from electrons and holes for appropriate use in the light propagation equations. In the direct term, an electron from a lower band absorbs a photon and transfers to a higher band.[22,37] The initial and final state wave vectors remain unchanged, but the final state energy is larger than the initial state energy by $\hbar\omega_0$. We have

$$\alpha_D = \left(\frac{2\pi e}{m}\right)^2 \left(\frac{1}{n\omega_0 c}\right) \sum_{\alpha\beta\mathbf{k}} f(E_\alpha^{\mathbf{k}}, E_f^{\alpha})[1 - f(E_\beta^{\mathbf{k}}, E_f^{\beta})] \times \left| \sum_j \langle \phi_\beta^{\mathbf{k}} | \mathbf{e}_j \cdot \mathbf{p} | \phi_\alpha^{\mathbf{k}} \rangle \right|^2 \delta(E_\beta^{\mathbf{k}} - E_\alpha^{\mathbf{k}} - \hbar\omega_0). \quad (7)$$

Since the energy separation between the LH and HH bands varies from 0 to several eV, this term is nonzero for hole-initiated FCA. However, the CBs are separated by energies

TABLE I. The TPA coefficients calculated with full bands are compared with those obtained using the analytical expression.

Parameters	λ (μm)	T (K)	β (analytical) (cm/MW)	β (our work) (cm/MW)
InAs	4.8	77	0.74	0.31
$Hg_{0.66}Cd_{0.34}Te$	4.8	77	2.09	1.37
InSb	9.6	77	1.66	0.81
$Hg_{0.76}Cd_{0.44}Te$	9.6	77	15.11	12.23
InAs	4.8	300	1.25	0.49
$Hg_{0.66}Cd_{0.34}Te$	4.8	300	1.63	1.04
InSb	9.5	300	8.37	3.30
$Hg_{0.76}Cd_{0.44}Te$	9.5	300	5.71	4.68

much larger than the usual photon energies of interest, and the direct excitation of electrons from the lowest CB to the next highest CB is not possible. Hence, in Eq. (7) both α and β denote valence bands and the FD function is evaluated with E_f^v. An additional mechanism to supply both momentum and energy is required for CB electrons to participate in the FCA. The most dominant contribution usually arises from longitudinal-phonon (LO) assisted FCA. Using the Frohlich Hamiltonian to describe electron-phonon interaction, the absorption coefficient for this indirect process can be written as

$$\alpha_{\mathrm{ID}}^{\pm} = \left[\frac{(2\pi)^3 e^4 \hbar\omega_{\mathrm{LO}}}{m^2 \hbar c (\hbar\omega)^3}\right]\left(\frac{1}{\kappa_\infty} - \frac{1}{\kappa_0}\right)\sum_{\alpha\beta\mathbf{k}} f(E_\alpha^{\mathbf{k}}, E_f^\alpha) \times \sum_{\mathbf{q}} [1 - f(E_\beta^{\mathbf{k}\pm q}, E_f^\beta)] R_{\alpha\beta}^{\mathbf{kq}} \delta[E_\alpha^{\mathbf{k}} \pm \hbar\omega_{\mathrm{LO}} + \hbar\omega - E_\beta^{\mathbf{k}\pm\mathbf{q}}], \tag{8}$$

$$R_{\alpha\beta}^{\mathbf{kq}} = \left(N_{\mathrm{LO}} + \frac{1}{2} \mp \frac{1}{2}\right)\left|\left\langle \phi_\beta^{\mathbf{k}\pm\mathbf{q}} \left| \frac{e^{i\mathbf{q}\cdot\mathbf{r}}}{q} \right| \phi_\beta^{\mathbf{k}} \right\rangle \sum_j (\langle \phi_\beta^{\mathbf{k}} | \mathbf{e_j}\cdot\mathbf{p} | \phi_\alpha^{\mathbf{k}} \rangle - \langle \phi_\beta^{\mathbf{k}\pm\mathbf{q}} | \mathbf{e_j}\cdot\mathbf{p} | \phi_\alpha^{\mathbf{k}\pm\mathbf{q}} \rangle)\right|^2,$$

where the $\hbar\omega_{\mathrm{LO}}$ and N_{LO} are the LO phonon energy and phonon population, κ_0 and κ_∞ are the dielectric constant at zero and infinite frequency, and the $\pm$ sign denotes phonon absorption or emission. For the conduction electrons, the initial, intermediate, and final states will all be in the lowest CB, whereas for the holes, the initial and final states can be in either the LH or HH bands. The FD functions are evaluated using appropriate quasi-Fermi level depending on the bands that contribute to the absorption. The total FCA coefficient α_f is the sum of the two contributions given by Eqs. (7) and (8), and the FCA cross section for electrons (holes) $\sigma_{e(h)}$ is the ratio of the coefficient to the total electron (hole) density $N_{e(h)}$. Simply,

$$\alpha_f = \alpha_D + \alpha_{\mathrm{ID}}^{+} + \alpha_{\mathrm{ID}}^{-}, \qquad \sigma_{e(h)} = \frac{\alpha_f}{N_{e(h)}}. \tag{9}$$

The calculated rate for FCA by electrons, which has only the indirect term, is much smaller than that for the holes. The FCA coefficients for both electrons and holes were found to be proportional to the carrier density. Consequently, σ is independent of the carrier density. The calculated values of σ_e, σ_h, and the total cross section σ are plotted as a function of wavelength in Fig. 6 for intrinsic InAs and $Hg_{0.66}Cd_{0.34}Te$ alloys. As expected the electron contribution is much smaller than the hole contribution. The total cross section is small at shorter wavelengths because of the unavailability of holes at those energies in the HH band. Since the hole density is greater near the zone center, the FCA cross section increases with the photon wavelength. However, because of the reduced intermixing of symmetries in both LH and HH band states near the zone center, the dipole matrix element decreases (and reaches zero at the center). Consequently, the cross section reduces with further increase in wavelength.

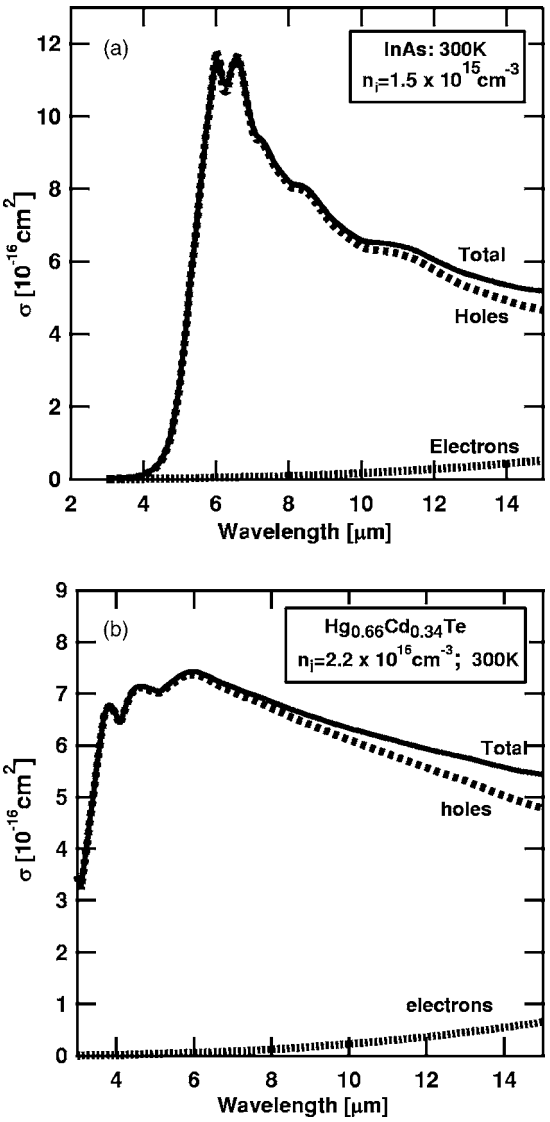

FIG. 6. Wavelength-dependent free carrier absorption cross section at 300 K.

The wavelength dependence of the FCA cross section in InSb and $Hg_{0.66}Cd_{0.34}Te$ alloys (not shown in here) is also similar.

When light energy is absorbed in semiconductors, equal densities of excited electrons and holes are created, which in turn release that energy to the lattice in the form of heat. To model light propagation through semiconductors, it is therefore necessary to know the FCA cross section as a function of both carrier concentration and temperature. The σ calculated for four materials as a function of wavelength at two temperatures are shown in Fig. 7. In the literature σ is usually assumed to be independent of temperature T. However, Fig. 7 shows that σ varies strongly with T—at long wavelengths, σ decreases with T, while at short wavelengths, it increases with T. This dependence can be explained by examining the transition rate obtained using the second-order perturbation theory. The absorption coefficient is approximately the integrated product of the hole density and optical matrix element. Although this coefficient is divided by the total hole density to get σ, only a fraction of the holes par-

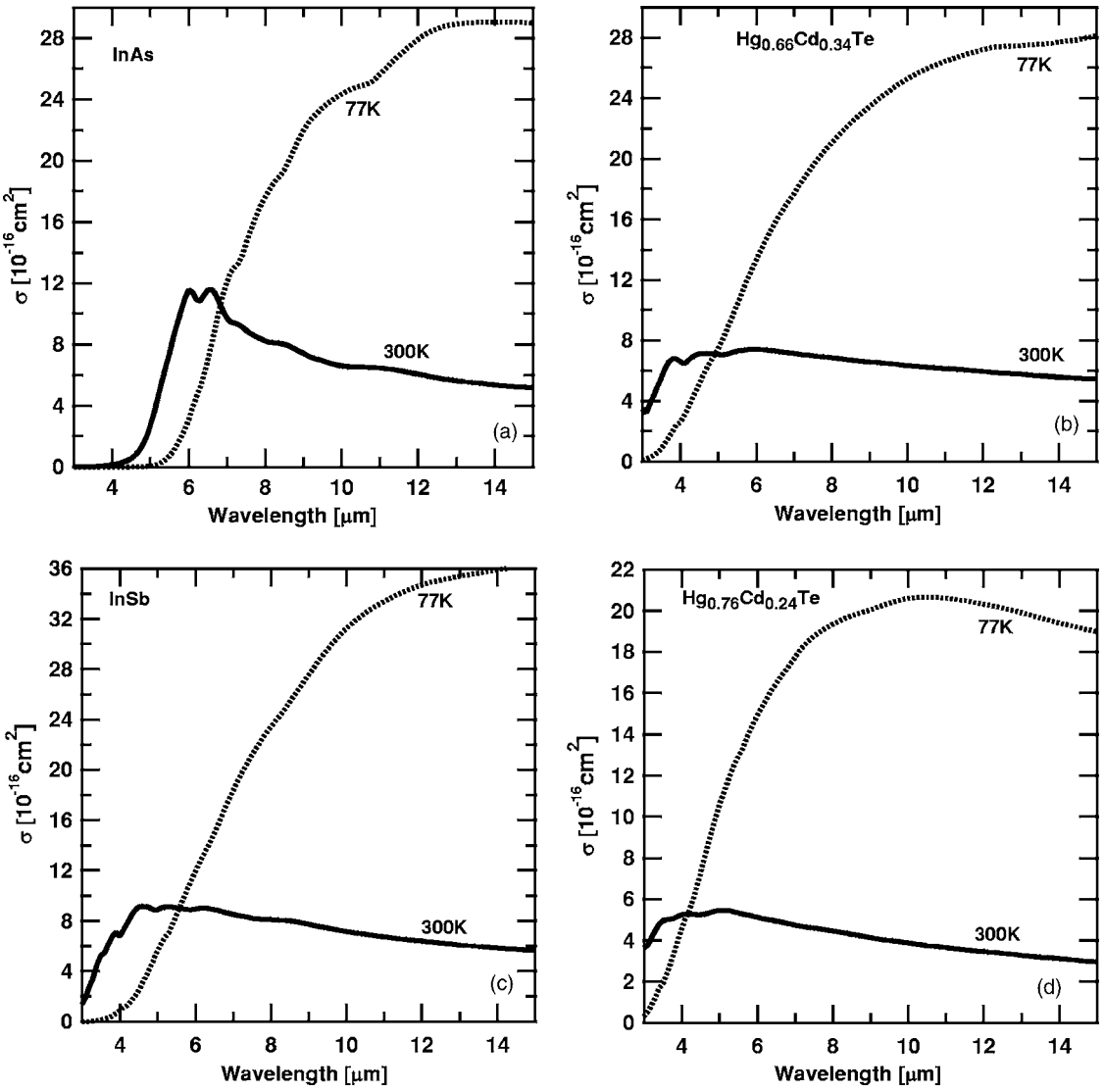

FIG. 7. Wavelength-dependent free carrier absorption cross section at 77 and 300 K.

ticipate in the absorption process because of energy and momentum conservation conditions. Even when the matrix elements do not change with T, the ratio of participating holes to the total number of holes has a strong dependence on T. For larger photon energies (or shorter wavelengths), the VB states away from the zone center participate in absorption and the hole density in those states increases with T. For longer wavelength photon absorption, the holes near the zone center participate and the hole density decreases with T as the holes are thermally excited to higher energies. Consequently, σ decreases with T.

We have calculated the T dependence of σ in InAs and $Hg_{0.66}Cd_{0.34}Te$ at a wavelength of 4.8 μm and in InSb and $Hg_{0.76}Cd_{0.24}Te$ at a wavelength of 9.6 μm. Figure 8 shows that the σ at 9.6 μm decreases by a factor of 14–16 as the T is increased from 77 to 500 K. σ at 4.8 μm in $Hg_{0.66}Cd_{0.34}Te$ is nearly a constant, but increases rapidly with T in InAs. It is important to note that the T dependence of σ is, in general, very strong except at one or two wavelengths where the hole density does not change with T.

The wavelength dependence of σ for various x values in $Hg_{1-x}Cd_xTe$ alloys are shown in Fig. 9 for (a) $T=300$ K and (b) $T=77$ K. As x increases, the band gap increases and the hole density decreases. Hence σ is expected to decrease

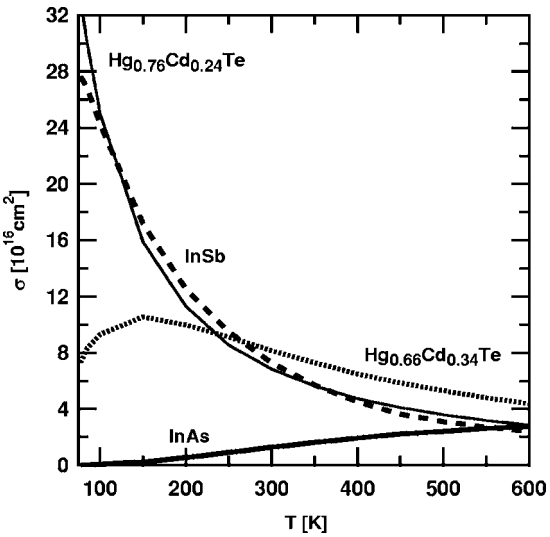

FIG. 8. Temperature-dependent free carrier absorption at 4.8 μm in InAs and $Hg_{0.66}Cd_{0.34}Te$ and at 9.6 μm in InSb and $Hg_{0.76}Cd_{0.24}Te$ at 300 K.

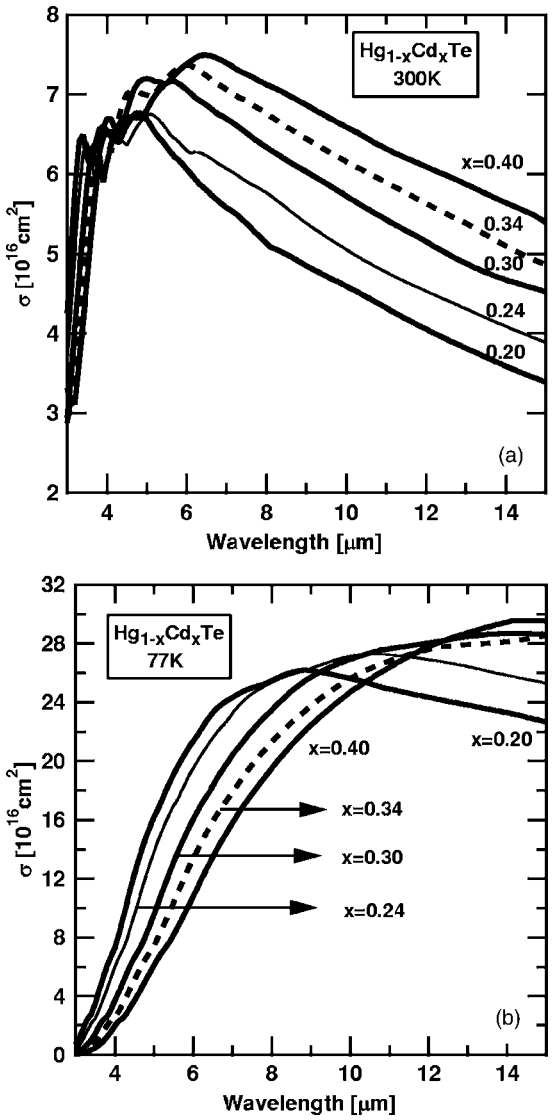

FIG. 9. Wavelength-dependent free carrier absorption cross section as a function of Cd concentration in HgCdTe alloys at (a) 300 K and (b) 77 K.

when x is increased. However, as x is increased, the spin-orbit coupling increases and the LH band bends more away from the HH band.[38] Consequently, the energy conservation condition is satisfied in the BZ closer to the zone center. This increases the density of participating holes, and hence, σ expected to increase with x is increased. The relative strengths of these two competing mechanisms depend on the wavelength and temperature. The crossover feature is seen clearly more at 77 K than at 300 K.

Lifetimes

The lifetimes τ of the excited electrons play a vital role in light propagation through the material because the excited carriers can participate in further absorption of light only before they recombine. The full band structures and accurate scattering matrix elements are used to obtain lifetimes as described previously.[25–27] Those calculations are here generalized to use the quasi-Fermi levels for electrons and holes. The lifetimes limited by the Auger recombination (AR) and radiative recombination (RR) are obtained as functions of temperature and carrier densities.

Parameter fit

Although the light propagation modeling studies[3–6,22,24] use only a few parameters—β, σ, τ, $N(=n_0+\Delta n)$, T, and sample thickness d—complications arise because of their interdependence. For example, β is a function of both N and T, but N depends on β and T. Similarly, τ depends on T and N, which in turn depends on T. Eventually, β, σ, and τ will determine the increase in T, which will in turn decide the values of those input parameters. Hence, for a self-consistent solution to the rate equations, it is preferable to have a closed functional form for the parameters β, σ, and τ, which is valid in the temperature and carrier density ranges of interest. The values of β and σ have been calculated at a wavelength of 4.8 μm in InAs and $Hg_{0.66}Cd_{0.34}Te$ and at 9.6 μm in InSb and $Hg_{0.76}Cd_{0.24}Te$, for $77\ \mathrm{K} < T < 500\ \mathrm{K}$ and $10^{14}\ \mathrm{cm}^{-3} < \Delta n < 10^{18}\ \mathrm{cm}^{-3}$. They are then fitted to the following expressions:

$$\beta(\mathrm{cm/MW}) = \frac{a}{1+\exp[(n-c)/b]}, \quad a = \sum_{i=0}^{4} a_i T^i,$$
$$b = \sum_{i=0}^{4} b_i T^i, \quad c = \sum_{i=0}^{4} c_i T^i, \tag{10}$$
$$n = (N \times 10^{-18}),$$

$$\sigma(10^{-16}\ \mathrm{cm}^2) = \sum_{i=0}^{4} \sigma_i T^i, \tag{11}$$

$$\tau_{\mathrm{AR}}(\mathrm{ns}) = 10^{(g+18h)} n^h, \quad g = \sum_{i=0}^{4} g_i T^i, \quad h = \sum_{i=0}^{4} h_i T^i, \tag{12}$$

$$N_i(10^{15}\ \mathrm{cm}^{-3}) = e^{\tilde{n}}, \quad \tilde{n} = \sum_{i=0}^{4} \tilde{n}_i \left(\frac{1000}{T}\right)^i. \tag{13}$$

N is the total carrier density, which is the sum of n_0 and Δn (or p_0 and Δp for holes) in the unit of cm^{-3}. The parameters n, b, c, g, h, and $\tilde{n}$ are dimensionless. The parameters fitted to the calculated values are given in Table II for the four materials considered here. The table lists parameters only for AR lifetimes. We had previously calculated RR lifetimes and found them, in general, to be very long for these materials.[25] In addition, because of the photon recycling present in the thick samples studied here, the RR lifetimes are extremely long and have a negligible effect on light propagation. The fitted parameters for RR lifetimes are therefore not listed. The AR lifetimes in $Hg_{0.76}Cd_{0.24}Te$ are not calculated and not listed as they are not expected to be substantially different from those in $Hg_{0.66}Cd_{0.34}Te$.

TABLE II. The parameters used to fit the calculated β, σ, τ, and N_i at the wavelength of 4.8 μm for InAs and $Hg_{0.66}Cd_{0.34}Te$ and at 9.6 μm for InSb and $Hg_{0.76}Cd_{0.24}Te$, in the temperature range from 75 to 500 K and in the excited carrier density range from of 10^{14} to 10^{18} cm^{-3}.

Parameters	InAs	$Hg_{0.66}Cd_{0.34}Te$	InSb	$Hg_{0.76}Cd_{0.44}Te$
a_0	0.205 16	2.1620	2.5913	48.074
a_1	0.001 529 9	−0.003 947 30	0.003 969 1	−0.455 16
a_2	-1.859×10^{-6}	1.3372×10^{-5}	0.000 125 89	0.002 999 3
a_3	1.8466×10^{-9}	-3.1219×10^{-8}	-4.6698×10^{-7}	-8.3954×10^{-6}
a_4	3.4373×10^{-12}	3.3459×10^{-11}	6.6038×10^{-10}	7.718×10^{-9}
b_0	−0.034 375	0.117 42	−0.001 972 8	0.3932
b_1	0.002 064 5	0.000 413 77	0.000 312 68	−0.003 377 1
b_2	-2.1108×10^{-6}	5.3520×10^{-6}	5.2291×10^{-7}	2.0397×10^{-5}
b_3	-6.5561×10^{-10}	-6.6517×10^{-9}	7.3333×10^{-10}	-5.051×10^{-8}
b_4	5.6352×10^{-12}	5.4334×10^{-12}	3.0668×10^{-12}	4.563×10^{-11}
c_0	0.458 59	1.2756	−0.045 22	0.210 89
c_1	−0.001 353 4	−0.000 958 61	0.0	0.003 298 8
c_2	1.0666×10^{-5}	1.0237×10^{-5}	0.0	-3.8836×10^{-5}
c_3	-1.1906×10^{-8}	-1.8417×10^{-8}	0.0	1.1845×10^{-7}
c_4	4.3216×10^{-12}	-7.1237×10^{-12}	0.0	-1.1285×10^{-10}
σ_0	−2.8164	−0.955 01	46.1	65.296
σ_1	0.044 098	0.166 77	−0.2929	−0.571 62
σ_2	5.9962×10^{-6}	−0.000 813 82	0.000 826 67	0.002 110 9
σ_3	-2.2463×10^{-7}	1.4824×10^{-6}	-1.1092×10^{-6}	-3.4952×10^{-6}
σ_4	2.3863×10^{-10}	-9.422×10^{-10}	5.6047×10^{-10}	2.1284×10^{-9}
g_0	40.467	43.429	47.74	43.429
g_1	−0.027 37	−0.067 12	−0.152 05	−0.067 12
g_2	-8.597×10^{-6}	2.480×10^{-4}	0.000 752 8	2.480×10^{-4}
g_3	2.2386×10^{-7}	-3.7801×10^{-7}	-1.6296×10^{-6}	-3.7801×10^{-7}
g_4	-3.122×10^{-10}	1.8071×10^{-10}	1.241×10^{-9}	1.8071×10^{-10}
h_0	−2.1984	−2.3581	−2.5943	−2.3581
h_1	0.000 518 36	0.003 266 5	0.007 922 6	0.003 266 5
h_2	5.578×10^{-6}	-1.1833×10^{-5}	-4.0231×10^{-5}	-1.1833×10^{-5}
h_3	-2.2914×10^{-8}	1.7764×10^{-8}	8.9063×10^{-8}	1.7764×10^{-8}
h_4	2.5089×10^{-11}	-7.8921×10^{-12}	-6.8868×10^{-11}	-7.8921×10^{-12}
$\tilde{n}_0$	11.119	9.3877	10.305	8.605
$\tilde{n}_1$	−3.6906	−2.9946	−2.4768	−2.0477
$\tilde{n}_2$	0.155 58	0.154 55	0.092 403	0.164 55
$\tilde{n}_3$	−0.010 771	−0.010 242	−0.004 431 9	−0.010 89
$\tilde{n}_4$	0.000 296 32	0.000 264 68	8.7616×10^{-5}	0.000 280 82

EXPERIMENTS AND RESULTS

For samples that have a thickness that is smaller as compared to the collimated region of the laser beam incident on them, it can be assumed that the beam remains collimated even at high intensities. The equation describing the space and time evolution of the pump intensity I_P and probe beam intensity I_{pr} can be written as

$$\frac{dI_P}{dz} = -\beta I_P^2 - (\sigma_e N_e + \sigma_h N_h) I_p, \tag{14}$$

$$\frac{d(\Delta n)}{dt} = \frac{\beta I_P^2}{2\hbar\omega} - \frac{\Delta n}{\tau_R}, \tag{15}$$

$$\frac{dI_{pr}}{dz} = -(\sigma_e N_e + \sigma_h N_h) I_{pr}. \tag{16}$$

The first term in Eq. (14) is from TPA and the second term is from FCA. N_e is the total electron density (which is the sum of n_0 and Δn), N_h is the total hole density (which is the sum of p_0 and Δp), and τ_R is the total recombination time limited by AR, RR, and Shockley-Read-Hall (SRH) mechanisms. For an intrinsic material, the FCA term can be simplified to $\sigma N I_p$. The change in the excited carrier density is a resultant of the gain from the TPA and the loss to the recombination as described in Eq. (15). The probe intensity is too small to cause TPA, and the rate equation for I_{pr} [Eq. (16)] contains only a FCA term. When the high intensity is absorbed either by TPA or by FCA, the absorbed energy is eventually transferred to the lattice as heat. The consequent change in the lattice temperature can be obtained from the rate equation:

$$\frac{dT}{dt} = \frac{\beta I_P^2}{c_V} + \frac{(\sigma_e^* N_e + \sigma_h^* N_h) I_P}{c_V}, \tag{17}$$

where c_v is the specific heat of the material. The indirect term in FCA should take into account the phonon-emission-induced increase and phonon-absorption-induced decrease in T. The modified cross section σ^* includes the difference in the emission and absorption contributions in the indirect term of the FCA, i.e., $\sigma_{e(h)}^* = (\alpha_D + \alpha_{ID}^+ - \alpha_{ID}^-)/N_{e(h)}$. However,

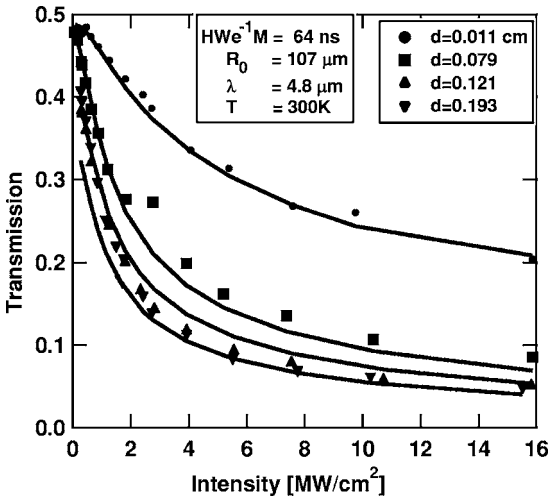

FIG. 10. Comparison of normalized pump transmission coefficient measured (data) at 300 K in 10^{15} n-doped InAs with that calculated (solid lines) for four thicknesses.

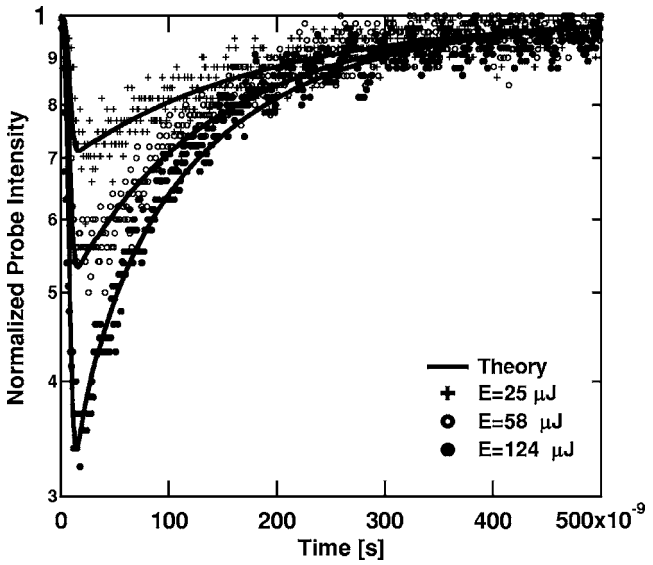

FIG. 11. Comparison of normalized probe transmission coefficient measured (data) at 300 K in 10^{15} n-doped InAs with that calculated (solid lines) for three beam energies.

the direct term in the FCA is considerably larger than the indirect term; the σ^* is nearly the same as σ. The parameters n_0, β, σ, and τ depend on T. In addition, β and τ_R depend on carrier density, which in turn depend on T. Hence Eqs. (14)–(17) will have to be simultaneously solved to find the I_P and I_{pr} at a time t and a position z in the sample.

We used the parameters for InAs listed in Table II and solved Eqs. (14)–(17) to explain the results obtained in our pump-probe experiment. Since the details are published elsewhere,[39] we discuss the results only briefly here to provide continuity. We set up a nonlinear energy transmission and a pump-probe experiment to determine the validity of the theory presented. In both experiments, a laser beam having a wavelength of 4.8 μm, obtained by frequency doubling a transverse excited atmospheric (TEA) CO_2 laser to provide 128 ns (full width at e^{-1} of the maximum) duration pulses with energies up to 10 mJ, was focused on InAs samples.

In the first experiment, the amount of energy incident on a set of samples of various thicknesses was varied and the ratio of the energy transmitted through the sample to the incident energy was plotted as a function of the incident intensity. Care was taken to ensure that the total energy transmitted by the samples was collected in the pyroelectric energy detectors by using a lens to focus the transmitted beam. The spatial distribution of the transmitted beam at various intensities was measured at the lens aperture and the lens of appropriate size was chosen so that the entire transmitted energy was collected. First, nonlinear absorption experiments were performed with only the pump present. The measured transmitted intensity as a function of incident intensity and sample thickness is shown in Fig. 10. As the intensity increased, more carriers are generated and the absorption increases, resulting in a decreased transmission. Similarly, as the thickness is increased, light is absorbed more. These trends are clearly observed. Also in Fig. 10, we have plotted the calculated transmitted intensity obtained from solving the rate equations [Eqs. (14)–(17)] with the values given in Table II. In addition to the Auger recombination, we have included lifetimes limited by the SRH mechanism. The SRH scattering is not intrinsic to the material and depends on external variables such as the growth temperature and pressure. Our detailed calculations carried out previously[40] indicate a nearly T-independent SRH lifetime of 200 ns in a 2×10^{16} cm^{-3} n-doped InAs. Although the InAs sample studied here is only 10^{15} cm^{-3} n doped, the excess carriers generated by the pump is of the order of $(1-2)\times10^{16}$ cm^{-3} and justifies the use of the above calculated SRH lifetimes. We further assumed that the SRH lifetime decreases linearly with excess carrier density. We see that the calculated transmission intensity agrees very well with measured values for all thicknesses studied.

In a second set of experiments, a weak continuous wave probe beam (at a wavelength of 5.3 μm) was made to be incident on the sample along with the pump beam (at 4.8 μm) and the temporal behavior of the probe beam was monitored as a function of the pump beam intensity. As the pump intensity increased, the probe beam power dropped because of the nonlinear absorption in the sample. However, at the end of the duration of the pump beam, i.e., after about 100 ns, the probe beam power recovered because of the decay of the free carriers, and the rate of recovery provided a measure of the carrier lifetime. In Fig. 11, the experimental data for the time dependence of the probe beam are presented for three values of the pump beam intensity, along with the theoretical calculations. It is seen that with only the SRH values used in an approximation, the time-dependent transmitted probe intensity calculated for the three input energies explains the observed variation very well.

CONCLUSIONS

We have used a full band structure, obtained from a hybrid pseudopotential tight-binding Hamiltonian, to calculate the temperature and carrier density dependent two-photon absorption coefficients, free carrier absorption cross section, and Auger lifetimes in InAs, InSb, and HgCdTe alloys. The accuracy of the calculations is enhanced with the use of the

quasi-Fermi levels, intrinsic carrier densities, detailed optical and scattering matrix elements, and complete integration over the entire BZ. The calculated parameters are fitted to closed-form functions and used in the rate equations to obtain the transmitted intensity as a function of time, incident intensity, and sample thickness. The nonlinear transmission calculated, with only the SRH lifetimes as an adjustable parameter, agrees very well the measured values. We showed that with accurate evaluation of all parameters, the modeling can provide detailed guidance in understanding the underlying mechanisms and in choosing materials for light propagation applications. The closed-form expressions for the fundamental parameters given here can be used in other accurate light propagation models.

ACKNOWLEDGMENTS

Two of the authors (S.K. and Z.G.Y.) gratefully acknowledge the funding from WPAFB Contract No. F33615-97-D-5403 through Anteon Corporation.

[1]L. W. Tutt and T. F. Boggess, Prog. Quantum Electron. **17**, 299 (1993).
[2]E. Garmire, IEEE J. Sel. Top. Quantum Electron. **6**, 1094 (2000).
[3]D. L. Kovsh, S. Yang, D. J. Hagan, and E. Van Stryland, Proc. SPIE **3472**, 163 (1988); Appl. Opt. **38**, 5168 (1999).
[4]J. Robertson, P. Milsom, J. Duignan, and G. Bourhill, Opt. Lett. **25**, 1258 (2000).
[5]J. Robertson, A. Smith, J. Duignan, P. Milsom, and G. Bourhil, Appl. Phys. Lett. **78**, 1183 (2001).
[6]E. Van Stryland, Y. Y. Wu, D. J. Hagan, M. J. Soileau, and K. Mansour, J. Opt. Soc. Am. B **5**, 1980 (1988).
[7]R. M. Grant, J. Opt. Soc. Am. **55**, 1457 (1965).
[8]R. M. Culpepper and J. R. Dixon, J. Opt. Soc. Am. **58**, 96 (1968).
[9]A. Miller, A. Johnson, J. Dempsey, J. Smith, C. R. Pidgeon, and G. D. Holah, J. Phys. C **12**, 4839 (1979).
[10]A. M. Johnson, C. R. Pidgeon, and J. Dempsey, Phys. Rev. B **22**, 825 (1980).
[11]M. H. Weiler, Solid State Commun. **39**, 937 (1981).
[12]B. S. Wherrett, J. Opt. Soc. Am. B **1**, 67 (1984).
[13]J. B. Doviak, A. F. Gibson, F. M. Kimmitt, and A. C. Walker, J. Phys. C **6**, 593 (1973).
[14]E. Van Stryland, M. A. Woodall, H. Vanherzeele, and M. J. Soileau, Opt. Lett. **10**, 490 (1985).
[15]M. S. Bahaei, P. Mukherjee, and H. S. Kwok, J. Opt. Soc. Am. B **3**, 379 (1986), and references cited therein.
[16]E. Van Stryland, H. Vanherzeele, M. A. Woodall, M. J. Soileau, A. L. Smirl, S. Guha, and T. Boggese, Opt. Eng. (Bellingham) **24**, 613 (1985).
[17]D. C. Hutchings and E. Van Stryland, J. Opt. Soc. Am. B **9**, 2065 (1992).
[18]B. N. Murdin, C. R. Pidgeon, A. K. Kar, D. A. Aroszynski, J.-M. Ortega, R. Prazeres, and F. Glotin, Opt. Mater. (Amsterdam, Neth.) **2**, 89 (1993).
[19]B. N. Murdin, C. Merviell, A. K. Kar, C. R. Pidgeon, D. A. Jaroszynski, J.-M. Ortega, R. Prazeres, and F. Glotin, Opt. Mater. (Amsterdam, Neth.), **2**, 89 (1993).
[20]K. W. Berryman and C. W. Rella, Phys. Rev. B **55**, 7148 (1997).
[21]M. B. Haeri, S. R. Kingham, and P. Milsom, J. Appl. Phys. **99**, 013514 (2006).
[22]S. Krishnamurthy, A. Sher, and A.-B. Chen, J. Appl. Phys. **88**, 260 (2000).
[23]S. Krishnamurthy, K. Nashold, and A. Sher, Appl. Phys. Lett. **77**, 355 (2000).
[24]A. Kobyakov, D. J. Hogen, and E. W. Van Stryland, J. Opt. Soc. Am. B **17**, 1884 (2000).
[25]S. Krishnamurthy, M. A. Berding, and Z. Yu, J. Electron. Mater. **35**, 1369 (2006).
[26]S. Krishnamurthy, A. Sher, and A.-B. Chen, J. Appl. Phys. **82**, 5540 (1997).
[27]S. Krishnamurthy and T. Casselman, J. Electron. Mater. **28**, 828 (2000).
[28]A.-B. Chen and A. Sher, *Semiconductor Alloys* (Plenum, New York, 1985), p. 233.
[29]S. Krishnamurthy, A. Sher, and A.-B. Chen, J. Electron. Mater. **24**, 1121 (1995).
[30]G. L. Hansen, J. L. Schmit, and T. N. Casselman, J. Appl. Phys. **53**, 7099 (1982).
[31]Z. Fang, K. Y. Ma, D. H. Jaw, R. M. Cohen, and G. B. Stringfellow, J. Appl. Phys. **67**, 7034 (1990).
[32]C. L. Littler and D. G. Seller, Appl. Phys. Lett. **46**, 986 (1985).
[33]S. M. Sze, *Physics of Semiconductor Devices* (Wiley, New York, 1981), p. 23.
[34]J. R. Meyer, C. A. Hoffman, F. J. Bartoli, D. A. Arnold, S. Sivananthan, and J. P. Faurie, Semicond. Sci. Technol. **8**, 805 (1993).
[35]I. Vurgaftman, J. R. Meyer, C. A. Hoffman, D. Redfern, J. Antoszewski, L. Faraone, and J. R. Lindemuth, J. Appl. Phys. **84**, 4966 (1998).
[36]C. H. Swartz *et al.*, J. Electron. Mater. **36**, 728 (2004).
[37]G. Shkerdin, J. Stiens, and R. Vounckx, J. Appl. Phys. **85**, 3792 (1999).
[38]Z. G. Yu, S. Krishnamurthy, and S. Guha, J. Opt. Soc. Am. B **23**, 2356 (2006).
[39]S. Krishnamurthy, Z. G. Yu, S. Guha, and L. Gonzalez, Appl. Phys. Lett. **89**, 161108 (2006).
[40]S. Krishnamurthy and M. A. Berding, J. Appl. Phys. **90**, 848 (2001).